Spring March 8, 2017

Multi-Color γ-Rays from Comb-Like Electron Beams Driven by Incoherent Stacks of Laser Pulses

Serge Y Kalmykov
X. Davoine, *CEA, DAM DIF*
Isaac Ghebregziabher, *The Pennsylvania State University*
Bradley A. Shadwick, *University of Nebraska - Lincoln*

Multi-color γ–rays from comb-like electron beams driven by incoherent stacks of laser pulses

S. Y. Kalmykov, X. Davoine, I. Ghebregziabher, and B. A. Shadwick

Citation: AIP Conference Proceedings **1812**, 100001 (2017); doi: 10.1063/1.4975899
View online: http://dx.doi.org/10.1063/1.4975899
View Table of Contents: http://aip.scitation.org/toc/apc/1812/1
Published by the American Institute of Physics

Multi-Color γ-Rays from Comb-Like Electron Beams Driven by Incoherent Stacks of Laser Pulses

S. Y. Kalmykov[1,a)], X. Davoine[2], I. Ghebregziabher[3] and B. A. Shadwick[1]

[1]*Department of Physics and Astronomy, University of Nebraska - Lincoln, Lincoln, NE 68588-0299, USA*
[2]*CEA, DAM, DIF, Arpajon F-91297, France*
[3]*Penn State Hazleton, PA 18202, USA*

[a)]Corresponding author: s.kalmykov.2013@ieee.org

Abstract. Trains of fs-length, GeV-scale electron bunches with controlled energy spacing and a 5-D brightness up to 10^{17} A/m^2 may be produced in a mm-scale uniform plasma. The main element of the scheme is an incoherent stack of 10-TW-scale laser pulses of different colors, with mismatched focal spots, with the highest-frequency pulse advanced in time. While driving an electron density bubble, this stack remains almost proof against nonlinear red-shift and self-compression. As a consequence, the unwanted continuous injection of background electrons is minimized. Weak focusing of the trailing (lower-frequency) component of the stack enforces expansions and contractions of the bubble, inducing controlled periodic injection. The resulting train of electron bunches maintains exceptional quality while being accelerated beyond the energy limits predicted by accepted scalings. Inverse Thomson scattering from this comb-like beam generates a sequence of quasi-monochromatic, fs-length γ-ray beams, an asset for nuclear forensics and pump-probe experiments in dense plasmas.

INTRODUCTION

Manipulations of the optical driver permit fine tuning of electron beam parameters in a laser-plasma accelerator (LPA) [1]. Using an incoherent stack of 10-TW-scale laser pulses, with a difference in frequency greater than 20%, is a promising way of extending the energy of quasi-monoenergetic (QME) electron beams without sacrificing their quality [2]. Advancing in time the high-frequency component of the stack compensates for the frequency red-shift imparted by electron blowout. This delays self-compression of the optical driver, preventing uncontrolled expansion of the electron density bubble and increasing, on average, the phase velocity of the bubble. This, in turn, reduces the amount of unwanted continuously injected charge and boosts electron energy far beyond the values predicted by accepted scalings [3]. In this way, GeV energy gain becomes possible, with high beam quality, in mm-length highly dispersive, dense plasmas ($n_0 \sim 10^{19}$ cm^{-3}), with a Joule-energy drive pulse [2]. This modest pulse energy offers the opportunity of high-repetition-rate operation at manageable average laser power, to the benefit of radiation physics applications critically dependent on dosage [4, 5]. High repetition rate also favors effective maintenance of the laser pulse quality (hence, of the electron beam quality) by using adaptive optics [6].

Controlled, background-free acceleration opens the way to further manipulations of electron beam phase space. Creating, in a single shot, a train of synchronized QME electron bunches with tunable energies is possible by propagating the stack in a plasma channel [2]. Periodic self-focusing of the stack tail causes oscillations in the bubble size and periodic injection of background electrons. The resulting comb-like beam has virtually no background [2]. Inverse Thomson scattering (ITS) [7, 8] from the comb-like beam produces multi-color γ-ray signal that consists of distinct bands of quasi-monochromatic radiation with tunable energy spacing [1, 9]. The mean energy of the bands is in the range of interest for nuclear forensics, 5–15 MeV [10]. Femtosecond-scale duration and synchronization of the γ-ray beams may also benefit pump-probe experiments in dense plasmas.

Here, we show that the plasma channel is not a prerequisite for generation of comb-like beams. The same effect may be achieved in the uniform plasma. The stacked driver with a weakly focused tail enforces the same periodic injection as previously observed in the channel. The resulting electron bunch train can drive the multi-color, pulsed γ-ray source based on the ITS, with a high number of photons ($> 10^6$) and 10 μJ-scale radiated energy.

Advanced Accelerator Concepts
AIP Conf. Proc. 1812, 100001-1–100001-5; doi: 10.1063/1.4975899
Published by AIP Publishing. 978-0-7354-1480-8/$30.00

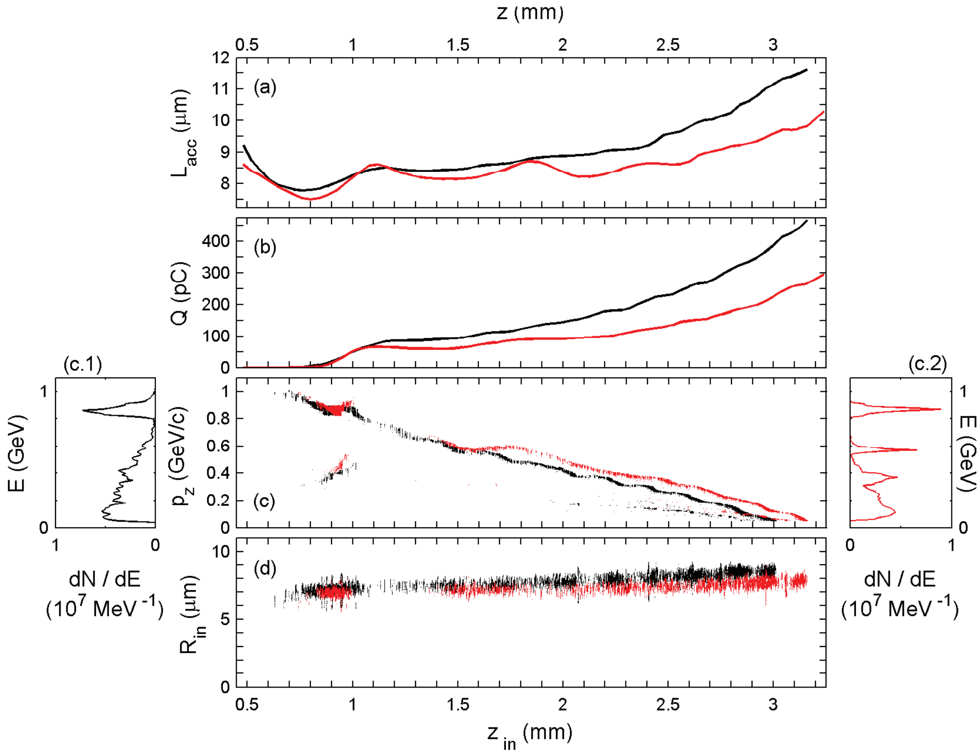

FIGURE 1. Generation of quasi-monoenergetic (case A, black) and comb-like electron beams (case B, red) in the uniform plasma. Panels (a) and (b) show the length of accelerating phase on axis (roughly, half-length of the bubble) and the charge of electrons with the energy above 50 MeV versus propagation distance. Electron charge in the bubble accumulates only during the intervals of bubble expansion. This is corroborated by the display of (c) collection phase space [final longitudinal momenta of electrons versus their initial positions] and (d) collection volume [initial radial positions versus initial longitudinal positions]. Corresponding energy spectra are shown in the sub-panels (c.1), (c.2). Weak focusing of the stack tail (case B) causes oscillation in the bubble size [seen in (a)], which results in the periodic injection and formation of the comb-like electron beam [panel (c.2)].

INTERACTION REGIMES AND SIMULATION METHODS

Manipulations of electron beam phase space are explored in particle-in-cell simulations using the relativistic, fully explicit, quasi-cylindrical code CALDER-Circ [11]. The code uses a numerical Cherenkov-free electromagnetic solver [12] and third-order splines for the macroparticles. These features, in combination with a fine grid ($\Delta z = \Delta r/16 = 0.125c/\omega_{\text{tail}} = 16$ nm, where $r^2 = x^2 + y^2$, and ω_{tail} is defined below) and large number of particles per cell (45), maintain low sampling noise, negligible numerical dispersion, and also avoid numerical emittance dilution.

The plasma begins at $z = 0$ with a 0.5 mm linear ramp, followed by the uniform section of the density $n_0 = 6.5\times10^{18}$ cm^{-3}. The total laser energy is 1.4 J, split equally between two linearly polarized, 35 TW pulses. These pulses are focused at the plasma border, and propagate towards positive z. The electric field in the focal plane is $\mathbf{E}_\perp(z=0) = \mathbf{E}_{\text{tail}} + \mathbf{E}_{\text{head}}$, where $|e|\mathbf{E}_{\text{tail}}/(m_e\omega_{\text{tail}}c) = \mathbf{e}_x\mathcal{E}_{\text{tail}}\exp[-i\omega_{\text{tail}}(t-T) - 2\ln 2(t-T)^2/\tau_L^2 - r^2/r_{\text{tail}}^2]$, and $|e|\mathbf{E}_{\text{head}}/(m_e\omega_{\text{tail}}c) = \mathbf{e}_y\mathcal{E}_{\text{head}}\exp(-i\omega_{\text{head}}t - 2\ln 2\, t^2/\tau_L^2 - r^2/r_{\text{head}}^2)$. Here, $-|e|$ and m_e are the electron charge and rest mass, c is the light speed in vacuum, $\mathbf{e}_{x,y}$ are unit polarization vectors, $\tau_L = 20$ fs, $T = 15$ fs, $\mathcal{E}_{\text{head}} = 2.31$, $r_{\text{head}} = 13.6$ μm, and $\omega_{\text{head}} = 1.5\omega_{\text{tail}}$. The stack components with carrier wavelengths $\lambda_{\text{tail(head)}} = 2\pi c/\omega_{\text{tail(head)}} = 0.805(0.54)$ μm are sufficiently overcritical to self-guide without an external plasma channel while maintaining electron blowout [3].

Frequency blue-shift of the head compensates for the red-shift imparted by blowout, making the stack immune to self-compression [2]. Nonlinear focusing and defocusing of the tail, which is sensitive to the ratio $R = r_{\text{tail}}/r_{\text{head}}$, controls variations in the bubble size, thus defining the number of QME components in the electron beam. Changing

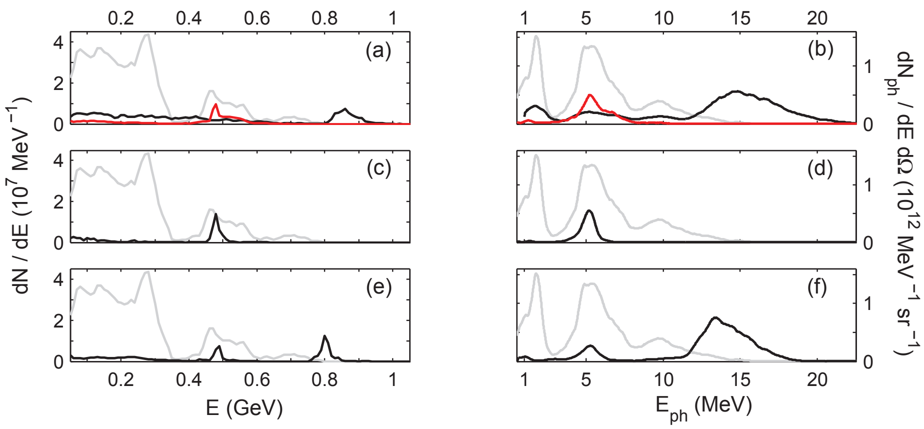

FIGURE 2. Progress through dephasing of the stacked pulse-driven LPA. Left column: electron energy spectra. Right column: ITS γ-ray spectra. (a), (b) Case A. Red (black) corresponds to electrons accelerated through $z = 1.67$ mm ($z_{\rm deph} = 3.11$ mm). Black in (c)–(f) corresponds to the case B. The highest energy electrons are accelerated through (c), (d) $z = 1.59$ mm, and (e), (f) $z = 2.63$ mm. Gray: the reference curves corresponding to the LPA driven with a transform-limited, 30 fs, 70 TW laser pulse, at dephasing ($z = 2.16$ mm) [9]. By comparison with the reference case, using the stacked driver with an overfocused tail [cf. (a), (b)] strongly reduces the low-energy background (in both electron and γ-ray signal). Alternatively, using the stack with a weakly focused tail compresses the remaining background into a second QME signal [cf. (e), (f)]. In all cases, the highest-energy electrons receive $\approx 70\%$ energy boost against the reference case, while the mean energy of the γ-rays triples.

R is thus one way to all-optically manipulate the electron phase space. In a uniform plasma, the stack with matched focal spots, $R = 1$ and $\mathcal{E}_{\rm tail} = \mathcal{E}_{\rm head} = 2.31$, drives the bubble very steadily. The resulting QME beam has an insignificant low-energy background and energy roughly 70% higher than expected from accepted scalings [2]. Here we show that overfocusing the tail (case A: $R = 1/\sqrt{2}$ and $\mathcal{E}_{\rm tail} = 3.27$) does not alter this dynamics. Conversely, weak focusing of the tail (case B: $R = \sqrt{2}$ and $\mathcal{E}_{\rm tail} = 1.63$) induces oscillations in the bubble size, creating a comb-like beam.

In the ITS simulations, macroparticles extracted from the first and second buckets of the wake sample the 6-D phase space of the electron beam. The beam is propagated in free space by solving the relativistic equations of motion and collides head-on with the linearly polarized interaction laser pulse (ILP) [13]. The centroid of the beam and the peak of the ILP intensity arrive at the ILP focal plane simultaneously. The ILP, specified analytically in the paraxial approximation, has a 0.8 μm carrier wavelength (photon energy $E_{\rm int} = 1.55$ eV), 250 fs duration (0.4% FWHM bandwidth), and 16.8 μm waist size (Rayleigh length 1.1 mm). As the ILP is shorter than 7% of its Rayleigh length and the electron beam spot size is in the sub-micron range, the interaction occurs in an almost plane-wave geometry.

For the relativistic and low-density beams considered here, $n_e \langle \gamma_e \rangle^{-3} \ll 10^{16}$ cm^{-3}, space charge forces are ne-

TABLE 1. Statistics of QME electron bunches at dephasing [Figs. 1(c.1) and 1(c.2); for the case B, see also Fig. 3(a)]. Q is the charge; $\langle E \rangle$ is the mean energy; σ_E is the energy dispersion; σ_τ is the root-mean-square (RMS) bunch duration; σ_α is the RMS divergence [2]; $\varepsilon_\perp^N$ is the RMS normalized transverse emittance [2]; $\langle I \rangle = Q/\sigma_\tau$ is the mean current; $B_n = 2\langle I \rangle (\pi \varepsilon_\perp^N)^{-2}$ is the 5-D brightness [18]; W is the total energy of the electron beam.

Units	Q pC	$\langle E \rangle$ MeV	σ_E MeV	σ_τ fs	σ_α mrad	$\varepsilon_\perp^N$ mm mrad	$\langle I \rangle$ kA	B_n A m^{-2}	W mJ
Case A	83.43	873.15	35.2	1.085	1.61	0.485	76.9	0.663×10^{17}	72.8
Case A, 2nd bucket	11.93	388.40	26.2	1.240	3.26	0.917	9.6	0.023×10^{17}	4.6
Case B, bunch I	57.70	873.00	21.25	0.735	1.45	0.407	78.6	0.960×10^{17}	50.4
Case B, bunch II	29.47	583.25	18.45	0.960	1.70	0.378	30.7	0.435×10^{17}	17.2
Case B, bunch III	64.15	383.15	54.45	2.410	3.44	0.718	26.6	0.105×10^{17}	24.6
Case B, 2nd bucket	3.10	453.35	33.65	0.810	2.85	0.512	3.8	0.030×10^{17}	1.4

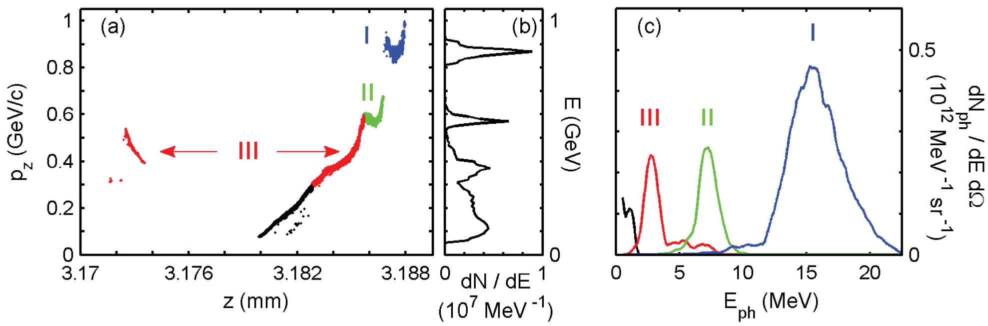

FIGURE 3. Longitudinal phase space (a) and energy spectrum (b) of the comb-like electron beam accelerated through dephasing in the case B. (c) ITS γ-ray signal split into partial signals from QME components (I)–(III) of the electron energy comb.

glected [14, 15]. Radiation damping is also neglected, as the energy emitted by an electron passing through the ILP is small compared to the electron energy. The interaction is in the linear regime [13, 16], with the ILP normalized vector potential $a_{\rm int}$ = 0.1. Once the orbits of individual electrons are obtained, and the energy radiated per unit frequency ω and solid angle Ω is calculated using classical formulas [17], averaging over the ensemble yields the mean radiated energy density per electron $d^2I_e/(d\omega d\Omega)$ [1]. The net energy radiated by the beam with a charge Q is $d^2I_{\rm tot}/d\omega d\Omega = (Q/|e|)d^2I_e/d\omega d\Omega$. Figures 2(b), 2(d), 2(f), and 3(c) show the photon flux per unit solid angle, in the direction of electron beam propagation (on-axis observation), in the plane of the ILP polarization.

RESULTS AND DISCUSSION

Figure 1 demonstrates that strong focusing of the stack tail (case A) preserves quasi-monoenergetic acceleration. Expansion and stabilization of the bubble between $z = 0.76$ and 1.52 mm creates a QME beam. By dephasing ($z_{\rm deph}$ = 3.11 mm), this beam absorbs 5.2% of the laser energy. From z = 1.67 mm [electron spectrum depicted in red in Fig. 2(a)] through dephasing [black in Fig. 2(a)], the slowly expanding bubble injects 250 pC, generating a weak continuous energy tail. Collection phase space [longitudinal momenta of electrons at $z = z_{\rm deph}$ versus their initial positions, Fig. 1(c)] and collection volume [initial radial positions versus initial longitudinal positions, Fig. 1(d)], corroborate this scenario of beam formation. As electron divergence in the tail is a factor 3 higher than in the QME component, the imprint of the tail on the ITS γ-ray signal is modest [cf. Fig. 2(b)]. The central energy of the dominant QME γ-ray signal may be thus safely tuned in the range of interest for nuclear photonics, 5–15 MeV [10]. A rather large, 19% energy spread of this signal (cf. Table 2) is imparted almost entirely by the 4% energy spread in the electron beam. This is proven in a pair of test ITS simulations. First, $p_z = \langle p_z\rangle = 1705 m_e c$ is assigned to all electrons while p_x and p_y are intact. This preserves the mrad-scale beam divergence, while almost zeroing out the energy spread. In the second run, the transverse momenta are set to zero, while p_z is intact, preserving the energy spread while zeroing out the divergence. The first run yields a monoenergetic ITS signal (sub-percent energy spread) centered at $E_{\rm ph} = 4\langle\gamma_e\rangle^2 E_{\rm int}$. Conversely, the photon signal from the second run still has $\approx$ 10% energy spread.

TABLE 2. ITS γ-rays emitted by the bunches with parameters specified in Table 1. $\langle E\rangle$ is the mean energy; σ_E is the energy dispersion; N_Ω and $W_\Omega = N_\Omega\langle E\rangle$ are the number of photons and energy radiated into the observation solid angle $\Omega = \pi\langle\gamma_e\rangle^{-2}$.

	$\langle E\rangle$ (MeV)	σ_E (MeV)	Ω (μsr)	N_Ω ($\times 10^6$)	W_Ω (μJ)
Case A	15.35	2.91	1.08	3.42	8.41
Case A, 2nd bucket	1.89	0.71	5.44	0.13	0.04
Case B, bunch I	15.77	2.48	1.08	2.49	6.27
Case B, bunch II	7.26	1.07	2.41	1.24	1.44
Case B, bunch III	2.79	0.55	5.60	2.30	1.28
Case B, 2nd bucket	3.00	0.91	4.00	0.02	0.01

In contrast to the case A, weak focusing of the stack tail (case B) results in an unbalanced self-focusing. This completely alters the kinetics of self-injection. Two oscillations in the bubble size seen in Fig. 1(a) generate a pair of QME bunches [beams I and II in Fig. 3(a)]. Their energy, through dephasing, is shown in Figs. 2(c) and 2(e). The ITS γ-ray spectra in Figs. 2(d) and 2(f) consist of a single- and a bi-color signals with virtually no background. Even though charge accumulates steadily after $z = 2.2$ mm, brief stabilization of the bubble around $z = 2.5$ mm monochromatizes the group of earlier injected particles, adding a third QME component to the energy comb [beam III in Fig. 3(a)]. By dephasing, the tri-color electron beam absorbs 6.55% of the laser energy. Statistics of the electron bunches and partial ITS γ-ray signals [cf. Fig. 3(c)] are summed up in Tables 1 and 2. Notably, the low-brightness beams from the second bucket contribute almost nothing to the ITS signal. Conversely, the bunches from the first bucket have the 5-D brightness $B_n = 2\langle I\rangle(\pi\varepsilon_{\perp,N})^{-2}$ reaching 10^{17} A/m^2, an order of magnitude higher than usually cited in the context of free-electron lasers and ITS-based light sources [18]. Hence a reasonably high number of photons (above 10^6) and a considerable energy (1.3–8.4 μJ) radiated in a μsr-scale observation solid angle $\Omega = \pi\langle\gamma_e\rangle^{-2}$. Using longer ILP may further increase the photon flux, while working with higher harmonics of ILP should boost the photon energy [8].

CONCLUSIONS

Photon engineering is a vital element of LPA design, offering new avenues to coherently control electron beam phase space on the femtosecond scale. One way to exercise this control is to synthesize the drive pulse by incoherently stacking collinearly propagating 10-TW-scale pulses of different wavelengths, with the blue-shifted pulse advanced in time to prevent self-compression of the driver. This approach is highly effective in boosting electron energy beyond the limits of accepted scalings without compromising beam quality. In addition, weak focusing of the trailing component of the stack enforces periodic injection, controllably producing synchronized sequences of ultra-bright, fs-length GeV-scale bunches, similar to those obtained in plasma channels [1, 9]. Inverse Thomson scattering from these clean comb-like beams produces polychromatic γ-ray beams with a sufficiently high photon flux. The natural mutual synchronization of fs-length electron bunches and γ-ray pulses may be an asset to nuclear pump-probe experiments.

ACKNOWLEDGMENTS

Work of SYK and BAS was supported by the NSF Grant PHY-1535678. Inverse Thomson scattering simulations were completed utilizing the Holland Computing Center (HCC) of the University of Nebraska. SYK expresses his cordial gratitude to Natasha Pavlovikj for her assistance in using the high-performance computing resources of HCC.

REFERENCES

1. S. Y. Kalmykov *et al.*, Plasma Phys. Control. Fusion **58**, 034006 (2016).
2. S. Y. Kalmykov *et al.*, Phys. Plasmas **22**, 056701 (2015).
3. W. Lu *et al.*, Phys. Rev. ST Accel. Beams **10**, 061301 (2007).
4. F. Albert *et al.*, Phys. Rev. ST Accel. Beams **13**, 070704 (2010).
5. L. Laschinsky *et al.*, J. Radiat. Res. **53**, 395 (2012).
6. Z.-H. He *et al.*, Nat. Commun. **6**, 7156 (2015).
7. N. D. Powers *et al.*, Nat. Photon. **8**, 28–31 (2014).
8. C. Liu *et al.*, Opt. Lett. **39**, 4132–4135 (2014).
9. S. Y. Kalmykov *et al.*, Nucl. Instrum. Methods Phys. Res. A **829**, 52–57 (2016).
10. S. G. Rykovanov *et al.*, J. Phys. B: At. Mol. Opt. Phys. **47**, 234013 (2014).
11. A. F. Lifschitz *et al.*, J. Comput. Phys. **228**, 1803–1814 (2009).
12. R. Lehe *et al.*, Phys. Rev. ST Accel. Beams **16**, 021301 (2013).
13. I. Ghebregziabher *et al.*, Phys. Rev. ST Accel. Beams **16**, 030705 (2013).
14. E. Esarey *et al.*, Phys. Rev. E **48**, 3003–3021 (1993).
15. S. K. Ride *et al.*, Phys. Rev. E **52**, 5425–5442 (1995).
16. P. Tomassini *et al.*, Appl. Phys. B: Lasers Opt. **80**, 419–436 (2005).
17. J. D. Jackson, *Classical Electrodynamics* (Wiley & Sons, Inc., 1999), p. 676.
18. A. Cianchi *et al.*, Nucl. Instrum. Methods Phys. Res. A **829**, 343–347 (2016).